MARTIN MARIETTA ENERGY SYSTEMS LIBRARIES

3 4456 0262430 0

ORNL/TM-10412

ornl

OAK RIDGE
NATIONAL
LABORATORY

MARTIN MARIETTA

Some Practical Considerations Involving Spectral Representations of 3-D Plasma Equilibria

S. E. Attenberger
W. A. Houlberg
S. P. Hirshman

OAK RIDGE NATIONAL LABORATORY
CENTRAL RESEARCH LIBRARY
CIRCULATION SECTION
4500N ROOM 175
LIBRARY LOAN COPY
DO NOT TRANSFER TO ANOTHER PERSON
If you wish someone else to see this report, send in name with report and the library will arrange a loan.

OPERATED BY
MARTIN MARIETTA ENERGY SYSTEMS, INC.
FOR THE UNITED STATES
DEPARTMENT OF ENERGY

Printed in the United States of America. Available from
National Technical Information Service
U.S. Department of Commerce
5285 Port Royal Road, Springfield, Virginia 22161
NTIS price codes—Printed Copy: A03; Microfiche A01

This report was prepared as an account of work sponsored by an agency of the United States Government. Neither the United States Government nor any agency thereof, nor any of their employees, makes any warranty, express or implied, or assumes any legal liability or responsibility for the accuracy, completeness, or usefulness of any information, apparatus, product, or process disclosed, or represents that its use would not infringe privately owned rights. Reference herein to any specific commercial product, process, or service by trade name, trademark, manufacturer, or otherwise, does not necessarily constitute or imply its endorsement, recommendation, or favoring by the United States Government or any agency thereof. The views and opinions of authors expressed herein do not necessarily state or reflect those of the United States Government or any agency thereof.

ORNL/TM-10412
Dist. Category UC-20g

Fusion Energy Division

SOME PRACTICAL CONSIDERATIONS INVOLVING SPECTRAL REPRESENTATIONS OF 3-D PLASMA EQUILIBRIA

S. E. Attenberger
Computing and Telecommunications Division
Martin Marietta Energy Systems, Inc.

W. A. Houlberg
S. P. Hirshman

Date Published–April 1987

Prepared by the
OAK RIDGE NATIONAL LABORATORY
Oak Ridge, Tennessee 37831
operated by
MARTIN MARIETTA ENERGY SYSTEMS, INC.
for the
U.S. DEPARTMENT OF ENERGY
under contract DE-AC05-84OR21400

MARTIN MARIETTA ENERGY SYSTEMS LIBRARIES
3 4456 0262430 0

CONTENTS

ABSTRACT v
1. INTRODUCTION 1
2. THE "INVERSE" TRANSFORMATION 2
3. MAGNETIC FIELD CALCULATION 4
4. TRACKING A CHORD 7
5. CHORDAL DATA INVERSION 14
6. CONCLUDING REMARKS 17
REFERENCES 19

ABSTRACT

For describing magnetically confined toroidal plasmas, it is convenient in some instances to use a cylindrical coordinate system whose origin is on the major axis of the torus and in others to use a "flux coordinate" system bound to the magnetic flux which is embedded in the plasma. A good estimate of the flux surface geometry is available in spectral form in many cases, permitting a simple transformation from flux coordinates to cylindrical coordinates. A modified Newton iteration is described for performing the "inverse" transformation from cylindrical coordinates to flux coordinates. An accurate technique for radial spline interpolation of the spectral coefficients is given which is particularly useful for computing magnetic fields near the magnetic axis.

Given a spectral representation of the plasma, it is possible to track a chord through the plasma, determining in sequence its intersections with a given set of flux surfaces. This technique is the starting point for many calculations, including neutral beam heating, pellet fueling, evaluation of absorption or plasma sources along the lines-of-sight of detectors, etc. An efficient algorithm for performing this calculation is given.

These algorithms permit the determination of plasma "profiles" from chordal data by a straightforward least-squares technique, without any restrictions on the orientation of the chords. The method shown is contrasted to those based on generalized Abel transforms.

1. INTRODUCTION

Let (R, ϕ, Z) be a cylindrical coordinate system whose origin is on the major axis of a magnetically confined toroidal plasma. (R is the major radius, ϕ is the toroidal angle, and Z is the distance above the midplane.) To relate flux surface quantities such as plasma density, temperature, etc., to cylindrical coordinates, we must also have another coordinate system, one that is embedded in the plasma. For convenience, we define the "flux coordinates" [1–4] $(\rho, \theta, \varsigma)$ as follows: θ is a poloidal coordinate, ς is a toroidal coordinate, and ρ is a radial coordinate labeling a flux surface defined by $\mathbf{B} \cdot \nabla \rho = 0$, where $\mathbf{B}$ is the magnetic field. Let

$$R(\rho, \theta, \varsigma) = \sum_m \sum_n R_{mn}(\rho) \cos(m\theta - n\varsigma) \ , \tag{1a}$$

$$Z(\rho, \theta, \varsigma) = \sum_m \sum_n Z_{mn}(\rho) \sin(m\theta - n\varsigma) \ , \tag{1b}$$

$$\phi(\rho, \theta, \varsigma) = \varsigma \ . \tag{1c}$$

Equations (1a) and (1b) are appropriate for plasmas that have vertical symmetry in at least two toroidal planes per field period (stellarator symmetry). This restriction, as well as the restriction that $\varsigma = \phi$, could be relaxed by extending the following analysis in a straightforward way.

In Section 2, we describe an iterative technique for the "inverse" transformation from (R, ϕ, Z) to $(\rho, \theta, \varsigma)$. We have chosen $\varsigma = \phi$ for computational convenience. Particular definitions of ρ and θ, which relate the flux coordinates to the magnetic field, are given in Sections 2 and 3, respectively.

The coefficients of the transformation (sometimes called "spectral coefficients") are generally given at a discrete set of ρ values by a magnetohydrodynamic (MHD) equilibrium code or by an algorithm that follows vacuum field lines. Splines can be used to interpolate the data in the ρ direction; special care is needed, however, in interpolating the data near the magnetic axis, particularly when computing the magnetic field. We show a way to reduce interpolation errors near the magnetic axis. In some cases, such as tracing rays that leave and reenter the plasma, extending the transformation beyond the plasma is useful. Because simple extrapolation of the splines works very poorly, a more robust (but still arbitrary) continuation of the transformation is given in Section 2. Section 3 lists the equations for the magnetic field in terms of the parameters chosen here and shows an example of errors in the field due to an inferior spline fit.

In Section 4 an efficient algorithm is described for finding, in sequence, the intersections of a straight trajectory with a set of nested flux surfaces. This algorithm builds on the techniques of Section 2 and forms the starting point for Section 5, which shows how plasma profiles may be determined from chordal data when the spectral coefficients are known.

2. THE "INVERSE" TRANSFORMATION

Given R, Z, and ϕ, we wish to compute the values of ρ and θ. Taylor-expanding R and Z about the approximate solution (ρ^k, θ^k) yields

$$R(\rho,\theta) = R^k + R_\theta^k(\theta - \theta^k) + R_\rho^k(\rho - \rho^k) + \cdots, \tag{2a}$$

$$Z(\rho,\theta) = Z^k + Z_\theta^k(\theta - \theta^k) + Z_\rho^k(\rho - \rho^k) + \cdots, \tag{2b}$$

where subscripts denote derivatives and where R^k and Z^k are the values obtained by evaluating Eqs. (1a) and (1b) at ρ^k and θ^k. Neglecting terms involving second and higher derivatives, we can solve Eqs. (2a) and (2b) simultaneously for ρ and θ at the $(k+1)$th iteration. The solution is

$$\theta^{k+1} = \theta^k + \frac{Z_\rho^k(R - R^k) - R_\rho^k(Z - Z^k)}{\tau^k}, \tag{3a}$$

$$\rho^{k+1} = \rho^k + \frac{R_\theta^k(Z - Z^k) - Z_\theta^k(R - R^k)}{\tau^k}, \tag{3b}$$

where

$$\tau = R_\theta Z_\rho - R_\rho Z_\theta \tag{4}$$

is the Jacobian of the transformation from (R, Z) to (ρ, θ). Note that derivatives with respect to θ and ς are available trivially from Eqs. (1a) and (1b), but derivatives with respect to ρ must typically be derived from spline fits of the $R_{mn}(\rho)$ and $Z_{mn}(\rho)$. This algorithm typically converges in two to six iterations with the error $|R^k - R| / R$ decreasing by about an order of magnitude per iteration. A poor initial guess costs only a couple of iterations in most cases. Convergence is said to be achieved when $(R^k - R)^2 + (Z^k - Z)^2 < \varepsilon_{\mathrm{I}}$, where ε_{I} is a small distance.

In pathological cases the $(k+1)$th iteration may give a worse result than the kth iteration. In that case the step size is halved, and an estimated mean value is used for the Jacobian as follows:

$$\theta^{k+2} = \theta^k + \frac{1}{2}\frac{Z_\rho^k(R - R^k) - R_\rho^k(Z - Z^k)}{0.75\tau^k + 0.25\tau^{k+1}}, \tag{5a}$$

$$\rho^{k+2} = \rho^k + \frac{1}{2}\frac{R_\theta^k(Z - Z^k) - Z_\theta^k(R - R^k)}{0.75\tau^k + 0.25\tau^{k+1}}. \tag{5b}$$

If necessary, the reduced step can be reduced again in a similar fashion. We have not observed any cases that fail to converge when treated in this way. Of course the problem could also be solved by using a library routine to find the zero of a function such as $F(\rho^k, \theta^k) = (R - R^k)^2 + (Z - Z^k)^2$. This is appropriate if a code must be

constructed quickly. However, for production work the method presented here is fast, robust, and straightforward. It has no unnecessary overhead and requires no adjustments to achieve optimal convergence.

Regardless of the iterative procedure used, special care is needed near the magnetic axis. To be specific, we must pick a definition of ρ. We let

$$\rho = (\Phi \,/\, \Phi_a)^{\frac{1}{2}} \ , \tag{6}$$

where Φ is the toroidal magnetic flux contained within a flux surface and Φ_a is the value of Φ at the plasma boundary. Then τ approaches zero at the magnetic axis and the transformation is undefined. If $\rho^k = 0$ but $(R^k, Z^k) \neq (R, Z)$, then we set $\rho^k = \rho_{\min}$ in order to proceed. Typically $\rho_{\min}$ is taken as ten times machine precision.

A related problem is that the quantities Z_ρ and R_ρ must be determined very accurately in the region where ρ is small to ensure a nonzero value for τ. It can be shown [1] that the $R_{mn}(\rho)$ and $Z_{mn}(\rho)$ are proportional to ρ^m as ρ approaches zero. To interpolate the data accurately, we factor out the dependence on ρ^m prior to performing the spline fit in ρ. We let

$$R\,(\rho, \theta, \varsigma) = \sum_m \sum_n \rho^m \widetilde{R}_{mn}(\rho) \cos\,(m\theta - n\varsigma) \tag{7a}$$

and

$$Z\,(\rho, \theta, \varsigma) = \sum_m \sum_n \rho^m \widetilde{Z}_{mn}\,(\rho) \sin\,(m\theta - n\varsigma) \ , \tag{7b}$$

where the quantities $\widetilde{R}_{mn}(\rho)$ and $\widetilde{Z}_{mn}(\rho)$ are the fitted functions. This form is particularly useful if the data are rather sparse near the axis. We will return to this point in the next section. Note that if data are not available at $\rho = 0$, a reasonable extrapolation from neighboring data points may be made using the ρ^m behavior.

In many practical applications, extending the transformation given by Eqs. (1a) and (1b) beyond the plasma is useful, even though the identification of ρ with magnetic flux surfaces may be meaningless for $\rho > 1$. A simple extension, which gives a unique mapping for plasma boundaries that are not too severely concave, is obtained as follows: let R_{10} and Z_{10} be proportional to ρ, and all other coefficients be constant for $\rho \geq 1$. This causes the flux surfaces to approach ellipses as $\rho \to \infty$. Note that a discontinuity in τ occurs at $\rho = 1$ using this algorithm. Equations (5a) and (5b) are very effective at dealing with a discontinuity in τ. Other treatments are possible. In particular, τ could be made continuous by causing the R_{mn} and Z_{mn} to be smooth functions of ρ. However, for applications such as tracking a chord to determine its intersections with a plasma (see Section 4), the computation of the additional spectral coefficients for $\rho > 1$ would slow down the calculation without increasing the accuracy.

3. MAGNETIC FIELD CALCULATION

The magnetic field associated with the flux coordinates $(\rho, \theta, \varsigma)$ can be written as [5,6]

$$\mathbf{B} = \frac{\nabla\Phi}{2\pi} \times (\nabla\theta^* - \iota\,\nabla\varsigma) \ , \tag{8}$$

where Φ is the toroidal magnetic flux, $\iota = \Psi'/\Phi'$, Ψ is the poloidal magnetic flux, primes denote derivatives with respect to ρ, and θ^* is the poloidal angle that makes the field lines "straight." To reduce the number of modes required to describe the transformation, we introduce the parameter λ, which satisfies

$$\theta^* = \theta + \lambda\,(\rho, \theta, \varsigma) \ , \tag{9}$$

where λ may be represented as

$$\lambda\,(\rho, \theta, \varsigma) = \sum_m \sum_n \rho^m \widetilde{\lambda}_{mn}(\rho) \sin\,(m\theta - n\varsigma) \tag{10}$$

and the coefficients of the expansion are determined along with those for R and Z by a steepest descent method [1]. The following discussion may, of course, be applied to straight-field-line coordinates by setting $\lambda = \lambda_\theta = \lambda_\varsigma = 0$. Equation (10) is appropriate for plasmas that have stellarator symmetry.

It can be shown that

$$\mathbf{B} = \frac{\Phi'}{2\pi R\tau}\left[(\iota - \lambda_\varsigma)\,\mathbf{e}_\theta + (1 + \lambda_\theta)\,\mathbf{e}_\varsigma\right] \ , \tag{11}$$

where $\mathbf{e}_\theta \equiv \partial\mathbf{x}\,/\,\partial\theta$ and $\mathbf{e}_\varsigma \equiv \partial\mathbf{x}\,/\,\partial\varsigma$ are covariant basis vectors. Given values for ρ and θ and assuming that Φ_a and $\iota(\rho)$ are known, we can solve for the magnetic field components using Eqs. (1a), (1b), (4), (6), (10), and (11). For convenience we list expressions for the cylindrical components of $\mathbf{B}$:

$$B^R = \frac{\Phi'}{2\pi R\tau}\left[(\iota - \lambda_\phi)\,R_\theta + (1 + \lambda_\theta)\,R_\phi\right] \ , \tag{12}$$

$$B^Z = \frac{\Phi'}{2\pi R\tau}\left[(\iota - \lambda_\phi)\,Z_\theta + (1 + \lambda_\theta)\,Z_\phi\right] \ , \tag{13}$$

$$B_{\rm tor} = \frac{\Phi'}{2\pi\tau}\,(1 + \lambda_\theta) \ . \tag{14}$$

Note that Φ' and τ both approach zero as $\rho \to 0$, so accurate determination of τ near the magnetic axis is critical in order to get sensible values for $\mathbf{B}$. Small errors in the R_{mn} and Z_{mn} data can cause large errors in the resulting $\mathbf{B}$ values near the axis, and thus careful determination of the equilibrium is required if the

magnetic field is to be reconstructed in this way. Figure 1 shows the importance of factoring out the ρ^m dependence prior to spline fitting the Fourier coefficients. For a typical tokamak geometry the flux surface quantity $RB_{\rm tor}$ (major radius times toroidal magnetic field) is plotted versus ρ near the magnetic axis. The solid line results from spline fitting the R_{mn}, Z_{mn}, and λ_{mn} coefficients. The dashed line corresponds to factoring out ρ^m prior to the spline fits. The open circles label $RB_{\rm tor}$ values corresponding to the knots of the splines. (In addition, there is a knot at $\rho = 0$, where the expression for $B_{\rm tor}$ is indeterminate.)

The magnetic field calculation described here has been used in numerical calculation of stellarator transport coefficients from the linearized drift Fokker-Planck equation, using equilibria generated by the 3-D MHD equilibrium codes MOMCON and VMEC [7,8]. Figure 2 shows mod(**B**) contours for the $\phi = \pi/4$ plane of the Advanced Toroidal Facility (ATF). The data for $R_{mn}(\rho)$, $Z_{mn}(\rho)$, $\lambda_{mn}(\rho)$, and $\iota(\rho)$ were available on a 31-point grid, uniformly spaced in ρ. An arbitrary set of flux surfaces (uniformly spaced in ρ) is shown by the dashed curves.

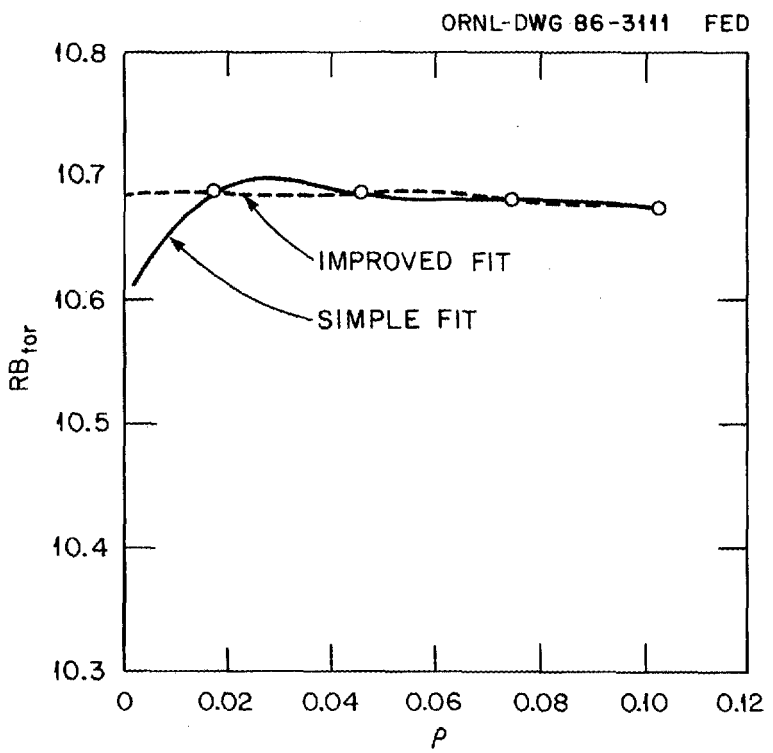

Fig. 1. Factoring out ρ^m prior to spline fitting the spectral coefficients improves the calculated value of the magnetic field near $\rho = 0$.

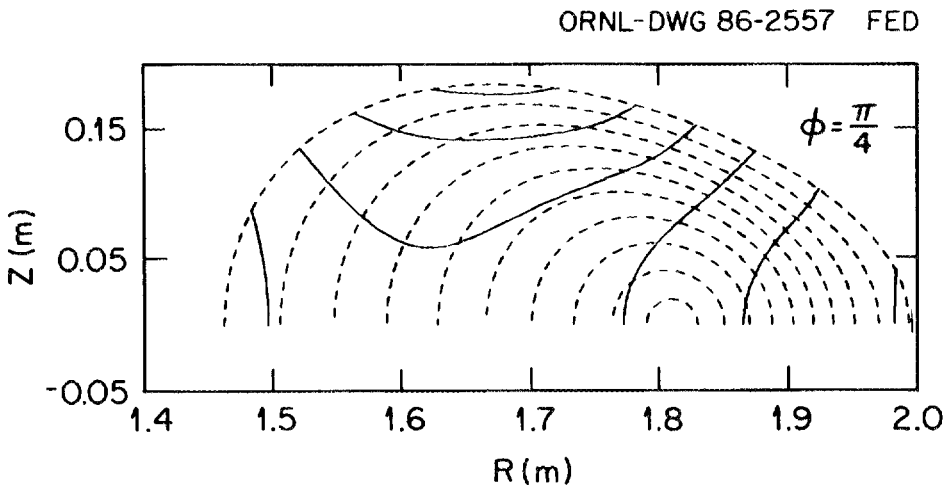

Fig. 2. Mod(**B**) contours.

4. TRACKING A CHORD

Suppose that we wish to find all the intersections of a straight trajectory with a given set of flux surfaces. Furthermore, they should be in the order in which they would be encountered when traveling along the trajectory. This is useful for such applications as neutral beam heating of plasmas. The fundamental technique is to take a step along the trajectory in such a way as to cross one and only one flux surface. Then the intersection with that flux surface corresponds to the zero of the function $\rho(S) - \rho_i$ on the interval (S^k, S^{k+1}), where S is the path length along the trajectory, ρ_i is the ρ value of the flux surface crossed, S^k is the start of the step, and S^{k+1} is the end of the step.

It may be shown that the variation of ρ along the trajectory satisfies

$$\rho'(S) \equiv \frac{\partial \rho}{\partial S} = \left[\frac{\partial \rho}{\partial R}\left(\frac{X}{R}\right) + \frac{\partial \rho}{\partial \phi}\left(-\frac{Y}{R}\right)\right]\frac{\partial X}{\partial S} + \left[\frac{\partial \rho}{\partial R}\left(\frac{Y}{R}\right) + \frac{\partial \rho}{\partial \phi}\left(\frac{X}{R^2}\right)\right]\frac{\partial Y}{\partial S} + \frac{\partial \rho}{\partial Z}\frac{\partial Z}{\partial S} \tag{15}$$

where S is path length along the trajectory and $(X = R\cos\phi, Y = R\sin\phi, Z)$ are Cartesian coordinates. Since the trajectory is straight in real space, the quantities $\partial X/\partial S$, $\partial Y/\partial S$, and $\partial Z/\partial S$ are constants along the trajectory. The remaining derivatives depend on the local Jacobian,

$$\frac{\partial \rho}{\partial R} = \frac{1}{\tau}\left(-\frac{\partial Z}{\partial \theta}\right) , \tag{16}$$

$$\frac{\partial \rho}{\partial \phi} = \frac{1}{\tau}\left(\frac{\partial R}{\partial \phi}\frac{\partial Z}{\partial \theta} - \frac{\partial R}{\partial \theta}\frac{\partial Z}{\partial \phi}\right) , \tag{17}$$

$$\frac{\partial \rho}{\partial Z} = \frac{1}{\tau}\left(\frac{\partial R}{\partial \theta}\right) . \tag{18}$$

Suppose that the plasma is divided into nested volume elements whose boundaries ρ_i are flux surfaces, where $0 \le \rho_i \le 1$. In addition, a dummy volume element $1 < \rho \le \rho_{\max}$ is defined to permit treatment of trajectories which lie outside of the plasma. At any point S^k on the trajectory one may determine $\rho^k \equiv \rho(S^k)$ and find the volume element in which S^k lies. Suppose that the surface ρ_i forms one of the boundaries of the current volume element. Then the path length to ρ_i is approximately

$$\Delta S_i^k = \left(\rho_i - \rho^k\right) / \rho'\left(S^k\right) . \tag{19}$$

Let ρ_i be the surface which makes $\Delta S_i^k > 0$. Then we attempt to span the intersection with ρ_i by taking a step $\Delta S^k = 1.1\Delta S_i^k$. Several tests are then performed to see whether one and only one surface has been spanned.

If $\rho^{k+1} = \rho\left(S^k + \Delta S^k\right)$ does not lie in the same volume element or an adjacent element, the step size is halved. However, the step size is required to be at least ε_S (the choice of ε_S is discussed later).

If $\Delta S^k > L_{\max}$ or $\Delta S^k > S_{\max}$ the step is truncated, where $S_{\max}$ is the length of the trajectory and $L_{\max}$ is chosen so that $\rho'(S)$ changes sign no more than once per step. Normally $L_{\max}$ can be set equal to the minor radius, but in highly rippled plasmas it should be less than the ripple spacing. Note that a change of sign in $\rho'(S)$ indicates that the trajectory is tangent to some surface ρ_T, which may or may not coincide with one of the ρ_i.

If $\rho'\left(S^{k+1}\right)$ has the opposite sign of $\rho'(S^k)$, then we find the zero of the function $\rho'(S)$ on the interval $\left(S^k, S^{k+1}\right)$ using the ZEROIN routine in a form similar to that presented by Forsythe, Malcolm, and Moler [9]. The step is shortened to fall at the solution point S_T, avoiding the possibility of missing a tangency point or a closely spaced pair of intersections when $\rho_T \approx \rho_i$.

If $\rho'(S)$ does not change sign but the step falls short of the surface ρ_i, then we set $S^k = S^{k+1}$ and recompute ΔS_i^k.

If none of the above conditions are met, then the step spans one and only one surface and we find the intersection $\rho(S) - \rho_i = 0$ on the interval $\left(S^k, S^{k+1}\right)$ using ZEROIN.

The ZEROIN procedure is required to converge within some tolerance $\Delta S < \varepsilon_Z$. After an intersection or a zero of $\rho'(S)$ has been found at some point S_Z, we check the sign of $\rho'(S_Z + \varepsilon_S)$ in order to find which surface the trajectory will approach next, and the procedure is repeated. The minimum step ε_S is necessary after an intersection in order to prevent finding the same intersection again when $S_i > S_Z \geq S_i - \varepsilon_Z$, where S_i is the exact position of the intersection. It is critical to maintain the relation $\varepsilon_S > \varepsilon_Z > \varepsilon_I$ among the minimum step size, the ZEROIN tolerance, and the inverse transformation tolerance. A reasonable choice is $\varepsilon_S = 2\varepsilon_Z = 200\varepsilon_I = L_{\max}/100$. [Note that $\rho(S)$ and $\rho'(S)$ must be obtained using a sequence of transformations $(X(S), Y(S), Z(S)) \rightarrow (R(S), Z(S), \phi(S)) \rightarrow (\rho(S), \theta(S), \phi(S))$, where the last transformation is the inverse transformation described in Section 2.]

Figure 3 shows the intersections of a set of nested flux surfaces with a trajectory in the $\phi = \pi/4$ plane of the ATF. The dotted lines are surfaces of constant θ. This case took less than 0.005 s of execution time per intersection on the CRAY-I for an equilibrium described by nine spectral modes. [See Eqs. (1a) and (1b).] This is typical for any trajectory (including trajectories that do not lie in a $\phi =$ constant plane), with execution time being roughly proportional to the number of modes.

In the modeling of neutral beam injection, it is useful to know the value of α, the angle between the particle trajectory and the magnetic field.

Note that

$$\cos\alpha = \frac{\mathbf{L}\cdot\mathbf{B}}{|\mathbf{L}|\,|\mathbf{B}|}\,, \tag{20}$$

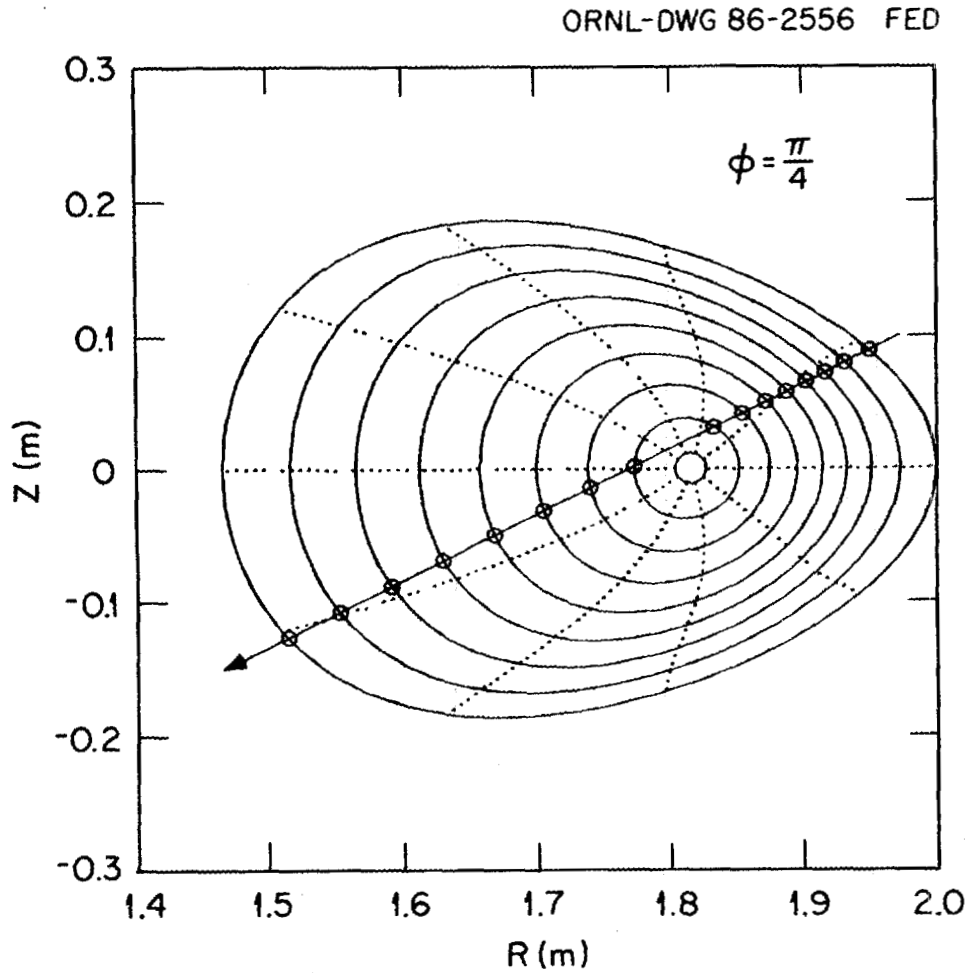

Fig. 3. Intersections of a straight line lying in a ϕ = constant plane with a set of flux surfaces.

where **L** is a path-length vector along the trajectory. This expression is most easily evaluated by converting the cylindrical components of **B** [Eqs. (12)–(14)] to the corresponding Cartesian components. Figure 4 shows $\cos\alpha$ as a function of path length for the trajectory in Fig. 3.

To illustrate the power of this technique, we consider a trajectory that intersects a Heliac plasma several times. Figure 5 shows a perspective view. It is helpful to compare it with Fig. 6, which shows a top view of the trajectory with the outline of the plasma and the magnetic axis. Figure 7 shows $\cos\alpha$ as a function of path length for this trajectory. Note that $\cos\alpha$ is not computed for those portions of the trajectory which lie outside of the plasma, since our data come from a fixed-boundary equilibrium code which does not model the magnetic field for $\rho > 1$.

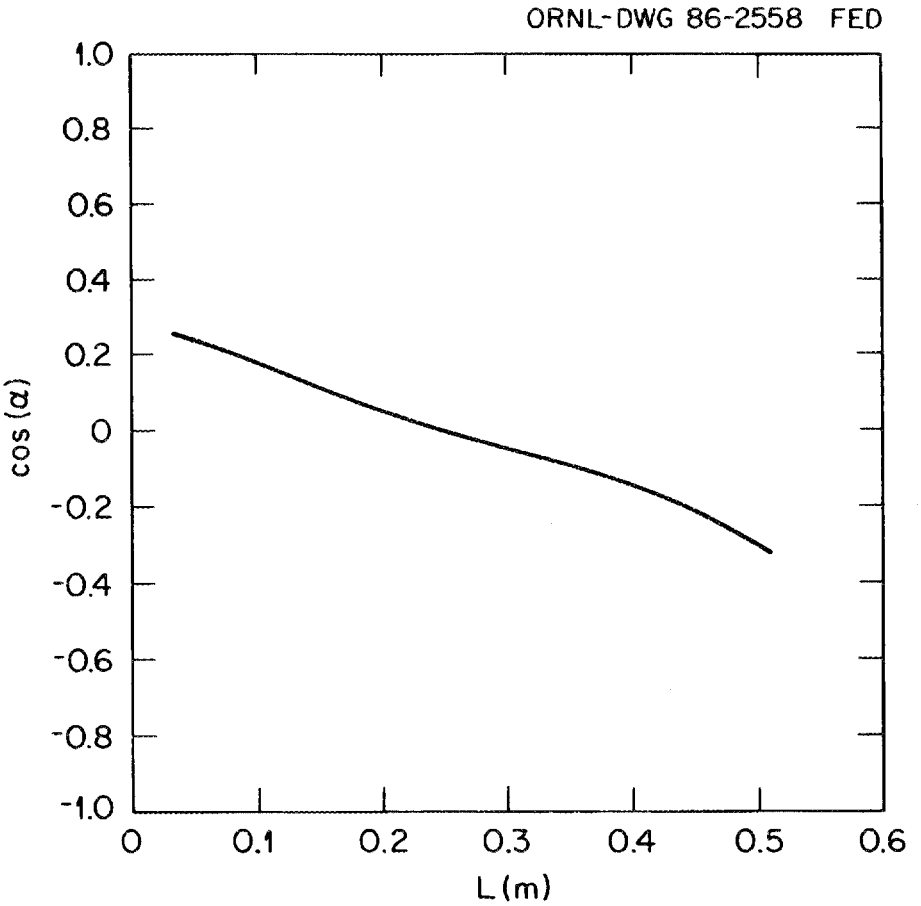

Fig. 4. Cos α vs path length along the trajectory.

ORNL-DWG 86-2559 FED

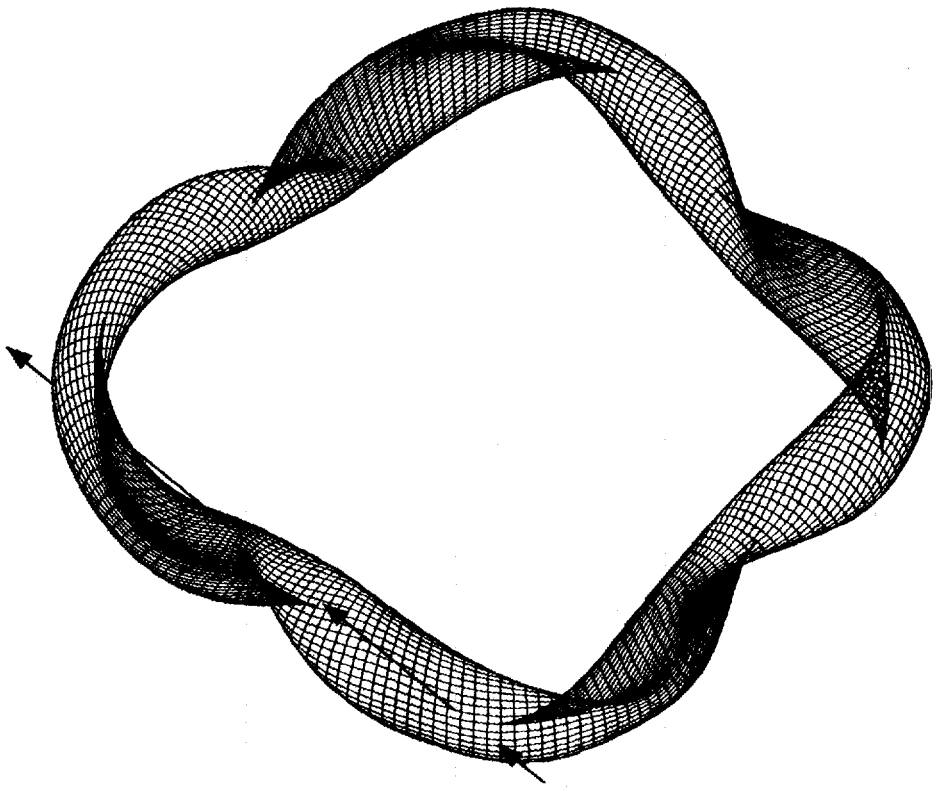

Fig. 5. Trajectory intersecting Heliac plasma multiple times (perspective view). The arrows show those parts of the trajectory which lie outside the plasma. The second arrow lies on the opposite side of the plasma from the viewer.

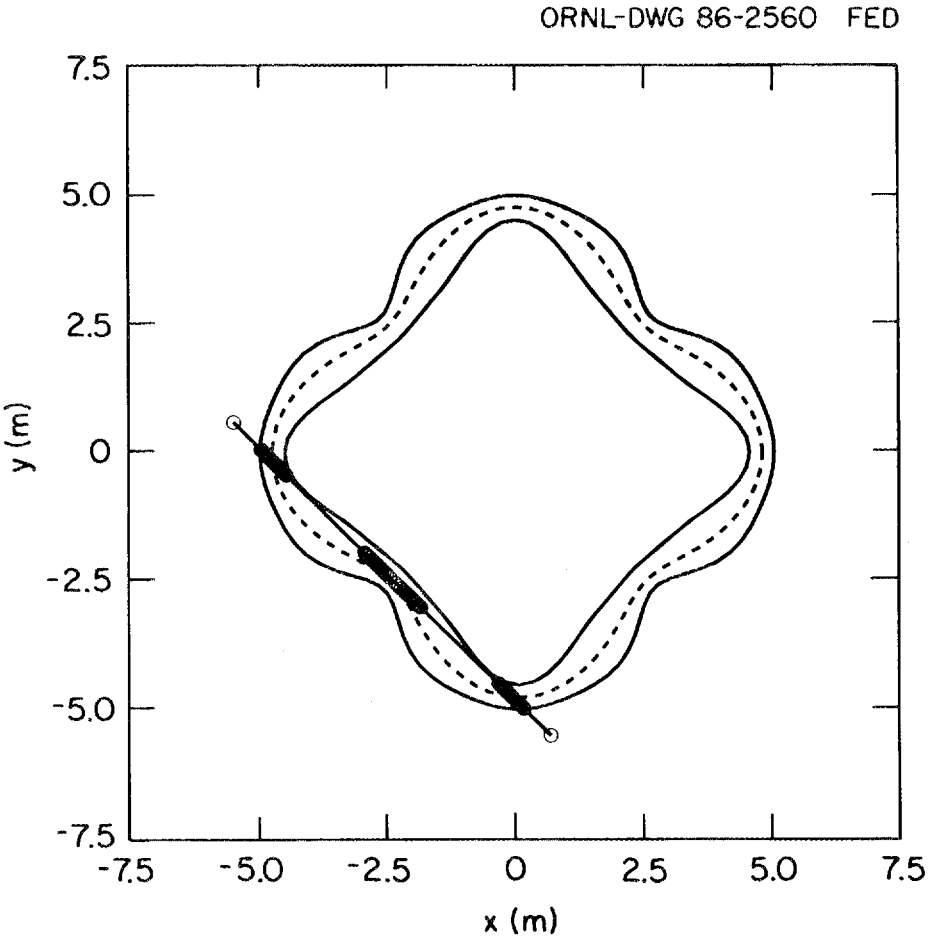

Fig. 6. Trajectory intersecting Heliac plasma multiple times (top view). The small circles indicate the ends of the trajectory and the intersections of the trajectory with a set of nested flux surfaces (not shown).

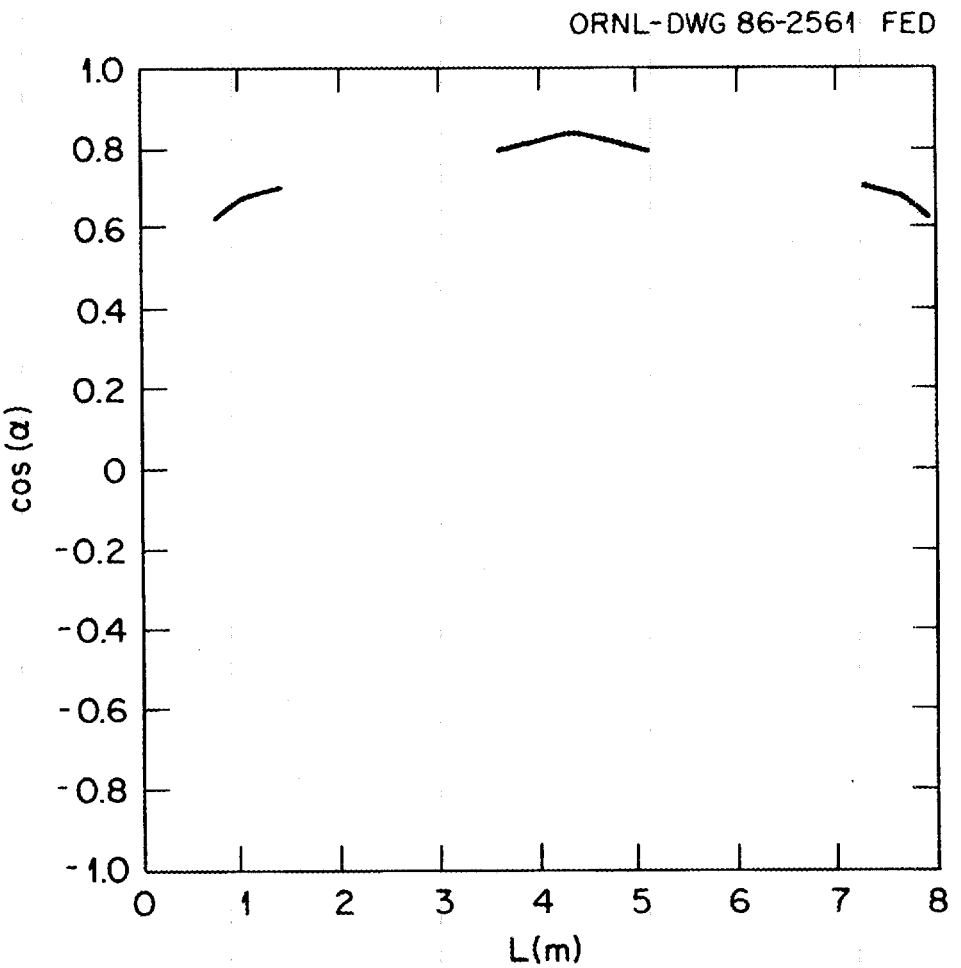

Fig. 7. Cos α versus path length along the trajectory.

5. CHORDAL DATA INVERSION

In a magnetically confined toroidal plasma, quantities such as density and temperature are nearly constant on a flux surface. Plots of these quantities as a function of ρ are called "profiles." A problem frequently encountered in experimental plasma physics is that of finding a plasma profile given measurements of absorption or source strength along a set of chords which are the lines of sight of an array of detectors. The measured values may be expressed as line integrals of some quantity which is constant on a flux surface. If the spectral coefficients in Equations (1a) and (1b) are known, the profiles may be determined by a straightforward least-squares method. Note that this is not the same as "Abel inversion" or the more general tomographic analysis of Granitz and Camacho [10], which do not assume any knowledge of flux surface shapes and which require the chords to lie in a plane at one toroidal position.

For example, suppose we want to know the bremsstrahlung source strength as a function of ρ. The experimental data are a set of photon counting rates from an array of collimated detectors. If S_k is the signal from the kth detector, then

$$S_k = f_k \int s(\rho)\, dL_k \ , \tag{21}$$

where f_k is a constant for the kth detector which includes the counting efficiency, L_k is path length along the kth chord, and $s(\rho)$ is the source strength in photons/m^3.

Assume that the source strength has the form

$$s(\rho) = \sum_j A_j s_j(\rho) \ , \tag{22}$$

where the A_j are constants and the $s_j(\rho)$ are a set of linearly independent functions that can be chosen to suit the purpose—for instance, polynomials, such as $s_1 = 1$, $s_2 = \rho$, and $s_3 = \rho^2$, or typical source profile shapes, such as $s_1 = \left(1-\rho^2\right)$, $s_2 = \left(1-\rho^2\right)^2$, etc. Substituting Eq. (22) into Eq. (21) gives

$$S_k = f_k \sum_j A_j G_{jk} \ , \tag{23}$$

where

$$G_{jk} \equiv \int s_j(\rho)\, dL_k \ . \tag{24}$$

Dividing the plasma into a set of nested volume elements whose boundaries are flux surfaces,

$$G_{jk} \simeq \sum_i s_{ij}\, \Delta L_{ik} \ , \tag{25}$$

where i is summed over all volume elements; s_{ij} is the mean value of $s_j(\rho)$ in the ith volume element; and ΔL_{ik} is the total path length of the kth chord in the ith volume element. The values ΔL_{ik} are obtained by finding the intersections of the kth chord with the set of flux surfaces as discussed in Section 4 and then simply computing the distance between intersections. For example, for three chords and two source terms we can write the set of equations from Eq. (23) as

$$\begin{pmatrix} G_{11} & G_{21} \\ G_{12} & G_{22} \\ G_{13} & G_{23} \end{pmatrix} \begin{pmatrix} A_1 \\ A_2 \end{pmatrix} = \begin{pmatrix} S_1 / f_1 \\ S_2 / f_2 \\ S_3 / f_3 \end{pmatrix} , \tag{26}$$

which can be solved in a least-squares sense for the A_j. Other treatments are possible. However, in all cases the starting point for the calculation is the determination of the intersections of the chords with a set of nested flux surfaces.

The method described here was used to study the evolution of the plasma density profile in Doublet III [11], although the reference mistakenly refers to the results as "Abel-inverted." The density profile was inferred from the bremsstrahlung source profile, which was computed from bremsstrahlung measurements taken at 1-ms intervals using 15 chords in a fan-shaped array. These chords were lying in the $Z = 0$ plane with at least one chord crossing the magnetic axis. The plasma was divided into nine volume elements for the analysis. In this configuration each volume element was intersected by at least one chord, permitting us to solve for a histogram of the source while making no assumptions about the form of the source profile. Formally, we have $s_j(\rho) = \delta_{ij}$ for $\rho_i \leq \rho < \rho_{i+1}$ where the ρ_i are the volume element boundaries. Inserting this into Eq. (25) yields $G_{jk} = \Delta L_{jk}$. Then A_j in Eq. (23) is the source strength in the jth volume element, and j is summed over volume elements.

After the histogram of the source was obtained, a 4-parameter fit was made using

$$N(\rho) = N(1) + a_1(1 - \rho^2) + a_2 \exp\left\{-\left[(\rho - a_3)/a_4\right]^2\right\} , \tag{27}$$

where N is the plasma density and the a_m were determined by a least-squares method. This represents a Gaussian perturbation to a smooth density profile caused by the injection of a pellet. Figure 8 shows a detail of the results of the calculation. A pellet was injected at about 560 ms. The perturbation broadens slowly as the density diffuses in both directions.

Other forms for the fit were also tried. Reference [11] shows the histogram itself, that is, the solution for the source profile evolution prior to obtaining a smooth fit. Although the chords in this example all lay in the midplane, in fact the orientation of the chords is arbitrary. The known geometry of the flux surfaces permits a simple solution for the source profile.

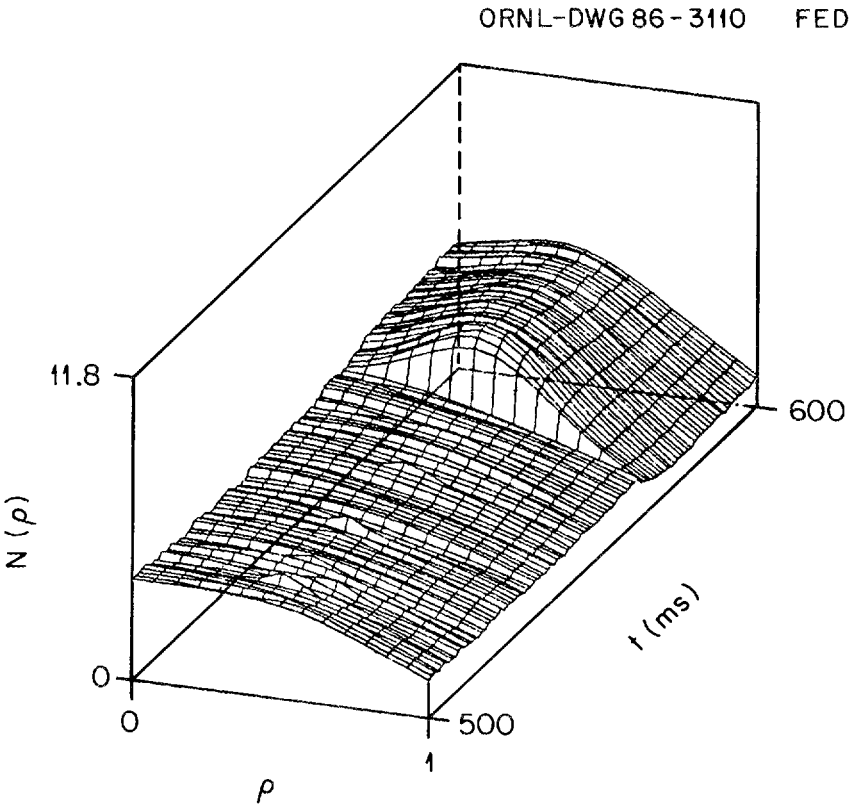

Fig. 8. Time-dependent density profile as inferred from chordal data during pellet injection into Doublet III.

6. CONCLUDING REMARKS

Spectral representations are currently in use in the data analysis codes of all major tokamak experiments and in many MHD equilibrium codes and tokamak transport codes. The recent emphasis on stellarator experiments is motivating the extension of existing two-dimensional techniques to more general geometries. The algorithms described here are fully three-dimensional and can be adapted easily to alternative definitions of the flux coordinates.

The authors will furnish a suite of FORTRAN subroutines containing these algorithms to interested parties. These routines have been tested and used in analysis of tokamak data from Doublet III and stellarator data from Heliotron E. Parts of the code are in use for transport simulation at Oak Ridge and Princeton. However, persons preferring to write or modify their own code should find that the algorithms are complete as described and that the programming effort required is not excessive.

REFERENCES

[1] S. P. Hirshman and J. C. Whitson, *Phys. Fluids* **26**, 3553 (1983).

[2] A. Bhattacharjee, J. C. Wiley, and R. L. Dewar, *Comput. Phys. Commun.* **31**, 213 (1984).

[3] L. Lao, *Comput. Phys. Commun.* **31**, 201 (1984).

[4] U. Schwenn, *Comput. Phys. Commun.* **31**, 167 (1984).

[5] M. D. Kruskal and R. M. Kulsrud, *Phys. Fluids* **1**, 265 (1958).

[6] S. Hamada, *Nucl. Fusion* **1**, 23 (1962).

[7] C. O. Beasley, J. A. Rome, S. E. Attenberger, and S. P. Hirshman, ORNL/TM-10222, to be published by Oak Ridge National Laboratory.

[8] S. P. Hirshman, K. C. Shaing, W. I. van Rij, C. O. Beasley, Jr., and E. C. Crume, Jr., *Phys. Fluids* **29**, 2951 (1986).

[9] G. E. Forsythe, M. A. Malcolm, and C. B. Moler, *Computer Methods for Mathematical Computations* (Prentice-Hall, New Jersey, 1977), p. 161.

[10] R. S. Granetz and J. F. Camacho, *Nucl. Fusion* **25**, 727 (1985).

[11] S. Sengoku et al., *Nucl. Fusion* **25**, 1475 (1985).

ORNL/TM-10412
Dist. Category UC-20 g

INTERNAL DISTRIBUTION

1–5. S. E. Attenberger
6. D. B. Batchelor
7. B. A. Carreras
8. E. C. Crume
9. R. H. Fowler
10. R. A. Dory
11. R. C. Goldfinger
12. J. H. Harris
13–17. S. P. Hirshman
18. J. T. Hogan
19–23. W. A. Houlberg
24. H. C. Howe
25. D. K. Lee
26. R. N. Morris
27. J. A. Rome
28. J. Sheffield
29. G. E. Whitesides
30. Laboratory Records, ORNL–RC
31. Document Reference Section
32. Central Research Library
33. Fusion Energy Division Library
34–35. Fusion Energy Division Publications Office
36. ORNL Patent Office

EXTERNAL DISTRIBUTION

37. G. Bateman, Princeton Plasma Physics Laboratory, P.O. Box 451, Princeton, NJ 08544
38. O. Betancourt, Courant Institute of Mathematical Sciences, New York University, 251 Mercer Street, New York, NY 10012
39. P. Garabedian, Courant Institute of Mathematical Sciences, New York University, 251 Mercer Street, New York, NY 10012
40. J. M. Greene, GA Technologies, Inc., San Diego, CA 92138
41. S. C. Jardin, Princeton Plasma Physics Laboratory, P.O. Box 451, Princeton, NJ 08544
42. W. Kerner, Courant Institute of Mathematical Sciences, New York University, 251 Mercer Street, New York, NY 10012
43. L. L. Lao, TO-512, GA Technologies, Inc., San Diego, CA 92138
44. K. M. Liang, Los Alamos National Laboratory, Los Alamos, NM 87545
45. J. Nührenberg, Max Planck Institute for Plasma Physics, D-8046 Garching, Federal Republic of Germany
46. D. E. Post, Princeton Plasma Physics Laboratory, P.O. Box 451, Princeton, NJ 08544
47. A. Schlüter, Max Planck Institute for Plasma Physics, D-8046 Garching, Federal Republic of Germany
48. U. Schwenn, Max Planck Institute for Plasma Physics, D-8046 Garching, Federal Republic of Germany
49. V. D. Shafranov, I. V. Kurchatov Institute of Atomic Energy, P.O. Box 3042, 123182 Moscow, U.S.S.R.

50. J. L. Shohet, Stellarator-Torsatron Laboratory, University of Wisconsin, Madison, WI 53706
51. A. M. M. Todd, Grumman Aerospace Corporation, 105 College Road East, Princeton, NJ 08540
52. M. L. Watkins, JET Joint Undertaking, Abingdon, Oxfordshire OX14 3DB
53. H. Weitzner, Courant Institute of Mathematical Sciences, New York University, 251 Mercer Street, New York, NY 10012
54. R. M. Wieland, Princeton Plasma Physics Laboratory, P.O. Box 451, Princeton, NJ 08544
55. Office of the Assistant Manager for Energy Research and Development Department of Energy, Oak Ridge Operations Office, P.O. Box E, Oak Ridge, TN 37831
56. J. D. Callen, Department of Nuclear Engineering, University of Wisconsin, Madison, WI 53706
57. J. F. Clarke, Director, Office of Fusion Energy, Office of Energy Research, ER-50 Germantown, U.S. Department of Energy, Washington, DC 20545
58. R. W. Conn, Department of Chemical, Nuclear, and Thermal Engineering, University of California, Los Angeles, CA 90024
59. S. O. Dean, Director, Fusion Energy Development, Science Applications International Corp., Gaithersburg, MD 20760
60. H. K. Forsen, Bechtel Group, Inc., Research Engineering, P.O. Box 3965, San Francisco, CA 94205
61. J. R. Gilleland, GA Technologies, Inc., Fusion and Advanced Technology, P.O. Box 85608, San Diego, CA 92138
62. R. W. Gould, Department of Applied Physics, California Institute of Technology, Pasadena, CA 91125
63. R. W. Gross, Plasma Research Library, Columbia University, New York, NY 10027
64. D. M. Meade, Princeton Plasma Physics Laboratory, P.O. Box 451, Princeton, NJ 08544
65. M. Roberts, International Programs, Office of Fusion Energy, Office of Energy Research, ER-52 Germantown, U.S. Department of Energy, Washington, DC 20545
66. W. M. Stacey, School of Mechanical Engineering, Georgia Institute of Technology, Atlanta, GA 30332
67. D. Steiner, Rensselaer Polytechnic Institute, Troy, NY 12181
68. R. Varma, Physical Research Laboratory, Navrangpura, Ahmedabad 380009, India
69. Bibliothek, Max-Planck Institut für Plasmaphysik, D-8046 Garching bei Munchen, Federal Republic of Germany
70. Bibliothek, Institut für Plasmaphysik, KFA, Postfach 1913, D-5170 Julich, Federal Republic of Germany
71. Bibliotheque, Centre des Recherches en Physique des Plasmas, 21 Avenue des Bains, 1007 Lausanne, Switzerland
72. F. Prevot, CEN/Cadarache, Department de Recherches sur la Fusion Controllée, F-13108 Saint-Paul-lez-Durance Cedex, France

73. Documentation S. I. G. N., Department de la Physique du Plasma et de la Fusion Controlee, Centre d'Etudes Nucleaires, B.P. 85, Centre du Tri, 38081 Grenoble, Cedex France
74. Library, Culham Laboratory, UKAEA, Abingdon, Oxfordshire, OX14 3DB, England
75. Library, FOM-Instituut voor Plasma-Fysica, Rijnhuizen, Edisonbaan 14, 3439 MN Nieuwegein, The Netherlands
76. Library, Institute of Plasma Physics, Nagoya University, Nagoya 464, Japan
77. Library, International Centre for Theoretical Physics, P.O. Box 586, I-34100 Trieste, Italy
78. Library, Laboratorio Gas Ionizatti, CP 56, I-00044 Frascati (Roma), Italy
79. Library, Plasma Physics Laboratory, Kyoto University, Gokasho, Uji, Kyoto, Japan
80. Plasma Research Laboratory, Australian National University, P.O. Box 4, Canberra, A.C.T. 2000, Australia
81. Thermonuclear Library, Japan Atomic Energy Research Institute, Tokai, Naka, Ibaraki, Japan
82. G. A. Eliseev, I. V. Kurchatov Institute of Atomic Energy, P. O. Box 3402, 123182 Moscow, U.S.S.R.
83. V. A. Glukhikh, Scientific-Research Institute of Electro-Physical Apparatus, 188631 Leningrad, U.S.S.R.
84. I. Shpigel, Institute of General Physics, U.S.S.R. Academy of Sciences, Ulitsa Vavilova 38, Moscow, U.S.S.R.
85. D. D. Ryutov, Institute of Nuclear Physics, Siberian Branch of the Academy of Sciences of the U.S.S.R., Sovetskaya St. 5, 630090 Novosibirsk, U.S.S.R.
86. V. T. Tolok, Kharkov Physical-Technical Institute, Academical St. 1, 310108 Kharkov, U.S.S.R.
87. Library, Academia Sinica, P.O. Box 3908, Beijing, China (PRC)
88. D. Crandall, Experimental Plasma Research Branch, Division of Development and Technology, Office of Fusion Energy, Office of Energy Research, ER-542 Germantown, U.S. Department of Energy, Washington, DC 20545
89. N. A. Davies, Office of the Associate Director, Office of Fusion Energy, Office of Energy Research, ER-51 Germantown, U.S. Department of Energy, Washington, DC 20545
90. D. B. Nelson, Director, Division of Applied Plasma Physics, Office of Fusion Energy, Office of Energy Research, ER-54 Germantown, U.S. Depart ment of Energy, Washington, DC 20545
91. E. Oktay, Division of Confinement Systems, Office of Fusion Energy, Office of Energy Research, ER-55 Germantown, U.S. Department of Energy, Washington, DC 20545
92. W. Sadowski, Fusion Theory and Computer Services Branch, Division of Applied Plasma Physics, Office of Fusion Energy, Office of Energy Research, ER-541 Germantown, U.S. Department of Energy, Washington, DC 20545
93. P. M. Stone, Fusion Systems Design Branch, Division of Development and Technology, Office of Fusion Energy, Office of Energy Research, ER-532 Germantown, U.S. Depart ment of Energy, Washington, DC 20545

94. J. M. Turner, International Programs, Office of Fusion Energy, Office of Energy Research, ER-52 Germantown, U.S. Depart ment of Energy, Washington, DC 20545
95. R. E. Mickens, Atlanta University, Department of Physics, Atlanta, GA 30314
96. M. N. Rosenbluth, RLM 11.218, Institute for Fusion Studies, University of Texas, Austin, TX 78712
97. Duk-In Choi, Department of Physics, Korea Advanced Institute of Science and Technology, P.O. Box 150, Chong Ryang-Ri, Seoul, Korea
98. Library of Physics Department, University of Ioannina, Ioannina, Greece
99. Theory Department Read File, c/o D. W. Ross, University of Texas, Institute for Fusion Studies, Austin, TX 78712
100. Theory Department Read File, c/o R. C. Davidson, Director, Plasma Fusion Center, NW 16-202, Massachusetts Institute of Technology, Cambridge, MA 02139
101. Theory Department Read File, c/o R. White, Princeton Plasma Physics Laboratory, P.O. Box 451, Princeton, NJ 08544
102. Theory Department Read File, c/o L. Kovrizhnykh, Lebedev Institute of Physics, Academy of Sciences, 53 Leninsky Prospect, 117924 Moscow, U.S.S.R.
103. Theory Department Read File, c/o B. B. Kadomtsev, I. V. Kurchatov Institute of Atomic Energy, P.O. Box 3402, 123182 Moscow, U.S.S.R.
104. Theory Department Read File, c/o T. Kamimura, Institute of Plasma Physics, Nagoya University, Nagoya 464, Japan
105. Theory Department Read File, c/o C. Mercier, Departemente de Recherches sur la Fusion Controlee, B.P. No. 6, F-92260 Fontenay-aux-Roses (Seine), France
106. Theory Department Read File, c/o T. E. Stringer, JET Joint Undertaking, Culham Laboratory, Abingdon, Oxfordshire OX14 3DB, England
107. Theory Department Read File, c/o R. Briscoe, Culham Laboratory, Abingdon, Oxfordshire OX14 3DB, England
108. Theory Department Read File, c/o D. Biskamp, Max-Planck-Institut fur Plasmaphysik, D-8046 Garching, Federal Republic of Germany
109. Theory Department Read File, c/o T. Takeda, Japan Atomic Energy Research Institute, Tokai Establishment, Tokai-mura, Naka-gun, Ibaraki-ken, Japan
110. Theory Department Read File, c/o L. D. Pearlstein, L-630, Lawrence Livermore National Laboratory, P.O. Box 5511, Livermore, CA 94550
111. Theory Department Read File, c/o R. Gerwin, CTR Division, Los Alamos National Laboratory, P.O. Box 1663, Los Alamos, NM 87545

112—252. Given distribution according to TIC-4500, Magnetic Fusion Energy (Category Distribution UC-20 g, Theoretical Plasma Physics)